Trophic level decoupling drives future changes in phytoplankton bloom phenology (79 characters with space)

Ryohei Yamaguchi[1,2 *], Keith B. Rodgers[1,2], Axel Timmermann[1,2], Karl J. Stein[1,2], Sarah Schlunegger[3], Daniele Bianchi[4], John P. Dunne[5], and Richard Slater[3]

[1] *Center for Climate Physics, Institute for Basic Science, Busan, South Korea*

[2] *Pusan National University, Busan, South Korea*

[3] *AOS Program, Princeton University, Princeton, NJ, United States*

[4] *Department of Atmospheric and Oceanic Sciences, University of California Los Angeles, Los Angeles, CA, United States*

[5] *NOAA/OAR Geophysical Fluid Dynamics Laboratory, NJ, United States*

***** Corresponding author: Ryohei Yamaguchi (ryamaguchi@pusan.ac.kr)

In preparation for *Nature Climate Change*

February 21th, 2022

Abstract

Climate change can drive shifts in the seasonality of marine productivity, with consequences for the marine food web. However, these alterations in phytoplankton bloom phenology (initiation and peak timing), and the underlying drivers, are not well understood. Here using a 30-member Large Ensemble of climate change projections, we show earlier bloom initiation in most ocean regions, yet changes in bloom peak timing vary widely by region. Shifts in both initiation and peak timing are induced by a subtle decoupling between altered phytoplankton growth and zooplankton predation, with increased zooplankton predation (top-down control) playing an important role in altered bloom peak timing over much of the global ocean. Light limitation is a primary control for bloom initiation changes only in limited regions. In the extratropics, phenological changes will exceed background natural variability by the end of the 21st century, which may impact energy flow in the marine food webs.

Main text

Marine primary productivity forms the basis of the marine food web and regulates the ocean's carbon cycle. The potential for climate change to have deleterious impacts on this productivity has received significant attention[1], motivating coordinated efforts to project and understand the long-term production capacity of marine ecosystems[2–4]. In addition to exploring future changes in mean productivity, it is also important to assess how the seasonal cycle of productivity will alter in response to anthropogenic forcing, as shifting phenology may have significant implications for natural and human systems. For example, changes in the seasonal timing of intense carbon fixation by primary producers at the base of the food web can affect predation, growth, and reproduction in higher trophic levels[5,6]. Such climate-driven mismatches can have further major impacts on local ecosystems[7] and fisheries[8], and thus on food security. To understand the adaptability of local ecosystems to climate change, and to develop sustainable strategies for human food production, model projections of when phenological changes will 'emerge' (the point in time at which the new characteristic state can be attributed to climate change) and what drives those changes are of tremendous utility.

There is less consensus regarding the drivers of future changes in the marine phenology of productivity than in the terrestrial analogue[9–13]. Over most extra-tropical oceans, the seasonal cycle is dominated by phytoplankton blooms, which are propelled by seasonal changes in environmental drivers (temperature, light, nutrient availability, grazing pressure, among others). Previous studies have suggested that onset of blooms and growing seasons have already shifted earlier in phase[7,14–17] and will continue to shift in the near future[18–21], especially at high latitudes. However, the mechanisms underlying such projected changes remain unresolved.

58 The complexity and diversity of environmental drivers that trigger, sustain, and curtail
59 phytoplankton blooms[22,23] complicate efforts to explore changing marine phenology.
60 Furthermore, there are also uncertainties in future projections of these drivers themselves[24].
61 Early efforts to explain climate-driven phenology shifts relied on the Sverdrup critical depth
62 paradigm[25], whereby the onset of blooms is mainly driven by increased light availability during
63 spring as the mixed layer shoals. Extending the critical depth hypothesis to anthropogenic
64 climate change, the early efforts argued that surface warming will lead spring stratification to
65 begin earlier, thereby modulating phytoplankton bloom timing as a "bottom-up" control[18,19].
66 On the other hand, recent studies have emphasized the importance of a more diverse set of
67 mechanisms that include reduced predation by zooplankton and a consequent increase in
68 phytoplankton accumulation[22,26–29], which constitute "top-down" controls. Given that these
69 abiotic and biotic environmental drivers tend to covary, simple correlation analysis cannot
70 deconvolve the underlying mechanisms.
71
72 In this study, we use the accumulation rate[30] of surface chlorophyll (Chl) to define the annual
73 phytoplankton bloom period as occurring from the beginning of Chl accumulation (bloom
74 initiation, Fig. 1a) to annual maximum of Chl (bloom peak timing, Fig. 1b). By further
75 assessing the budget for changes in the accumulation rate, we quantitatively attribute the
76 projected future change in bloom phenology (described in detail later and see also Methods).
77 This methodology disentangles bloom driver complexity and provides insights into the
78 underlying mechanisms as well as their responses to forced changes in the physical and
79 biological drivers[3,4] that modulate phenology.
80
81 Despite strong anthropogenic changes in many ocean properties impacting primary production
82 (e.g. temperature, mixing), analyses of Earth system model (ESM) simulations have shown

that anthropogenic trends on biological variables are relatively subtle, taking multiple decades to statistically emerge above background climate variability[31]. This underscores the value of a Large Ensemble framework, where one uses multiple realizations of the same model with identical forcing, but with different initial conditions, for isolating and attributing anthropogenic trends in marine biological variables. Here, we investigate future changes in phytoplankton bloom phenology via daily surface Chl, by far the most commonly observed bloom phenology variable, as well as other environmental variables (temperature, nutrient concentrations, light levels, among others) from a 30-member Large Ensemble simulation with the Geophysical Fluid Dynamics Laboratory Earth System Model 2 (GFDL-ESM2M[32–34], Methods) under a high-emissions scenario (historical/RCP8.5). The simulation realistically represents the main features of the seasonal cycle of sea surface Chl[35], i.e. phytoplankton bloom timing, as documented by comparisons with satellite records (Fig. S1–S4, Supplementary Note 1 and Extended Data Fig. 1).

Future projection of bloom phenology

Projected future changes in bloom initiation and peak timing reveal a complex response pattern (Fig. 1c and 1d). Overall, bloom initiation and peak timing trends are on the order of a few days per decade, but at the model-grid scale can be greater than one month over the course of the 21st century. Biome-averaged shifts provide insight into the broader-scale patterns of phenological change (Fig. 1e). Bloom initiation is expected to occur earlier in almost all biomes. Peak bloom is expected to be delayed in biomes across the Southern Ocean and Equatorial regions but shift earlier for all biomes in the Northern extra-tropical oceans. If we define the period from bloom initiation to bloom peak as the net growth period, the resulting changes in period length indicate that in the future, the ocean's "spring" will be shortened north of 30°N

(Fig. 1e). Such bidirectionality the timing of changes in bloom phenology implies a variety of drivers that vary by region and by season.

Future projected changes in bloom peak magnitude reveal more coherent spatial structures showing both increased and decreased bloom magnitude (Extended Data Fig. 2). In a biome-averaged perspective, bloom magnitude weakens in many Northern Hemisphere ocean regions except the high-productivity oceans of the subarctic North Pacific. In contrast, bloom peak magnitude increases for the Southern Ocean. This spatial pattern corresponds with the trend in annual mean sea surface Chl, which has been evaluated previously with the same model configuration[31], indicating that changes in blooms, which occur intermittently over a limited part of the annual cycle, play an important role in determining the mean state trend.

Many regional phenological changes are expected to emerge sometime prior to 2100 (indicated by stars in Fig. 1e). The Time of Emergence (ToE) indicates the point in time at which the forced change (ensemble mean) in bloom timing exceeds the trends that could be caused by natural variability alone (see Methods). Given that prey (e.g., plankton) and predators (e.g., fish larvae) have co-evolved and thus have interdependent phenology[6,36], a phytoplankton phenology shift occurring on the timescale of decades but exceeds historical year-to-year natural variability represents a significant perturbation that could cause a mismatch between prey and predator lifecycles[8,18], although predators may be able to adapt to such a shift, for example by migrating. In the context of ecosystems, ToE may represent a threshold for when phytoplankton phenology could induce phenological mismatch with consequences for the local ecosystem. Our results document an elevated risk of such mismatch especially in the Northern Hemisphere high latitudes, where ocean regions are characterized by high productivity and significant effects of rapid climate change.

At present, the observed trend in biome-averaged bloom characteristics is within the natural variability range estimated by the Large Ensemble (Extended Data Fig. 1), illustrating the challenge in detecting phenological changes from localized observations over the satellite ocean color record, as previously noted for bloom magnitude modulation[19,37]. Thus, in the coming decades, sustained observational efforts will be necessary, as will more refined statistical methods such as optimal fingerprinting[38], which may be more adept at separating anthropogenic change from natural variability. The phenological change's earliest expected emergence will occur in the Northern Hemisphere ice biome (N_ICE, Extended Data Fig. 1a), associated with the commonly projected rapid retreat of sea ice[39]. In these areas, both bloom initiation and bloom peak will shift earlier, emerging during the first half of the 21st century, with relatively larger shifts in the bloom peak timing resulting in compression of the net growth period.

Mechanistic drivers of phenological change

The time rate of change in the Chl accumulation rate (r, day^{-1}, the indicator of phytoplankton bloom in this study) is determined by phytoplankton's growth rate (μ, day^{-1}) and loss rate (l, day^{-1}) (including cell division, predation by zooplankton, aggregation, mortality, etc.); changes in the chlorophyll-carbon ratio (Chl:C, θ, photo-acclimation, the physiological response of phytoplankton); and a dilution effect due to surface mixed layer (ML, h) deepening (See also Methods):

$$r \equiv \frac{1}{Chl}\frac{d\,Chl}{dt} \approx \mu - l + \frac{d\ln(\theta)}{dt} - \frac{d\ln(h)}{dt}. \quad (1)$$

Phytoplankton variables (μ, l, and θ) are summed over the three phytoplankton groups (small, large, and diazotrophic phytoplankton), after weighting by each group's abundance (Equation M4 in Methods). Note that Equation 1 requires that, over the spatial and temporal scales this

study investigates, advection and diffusion play minor roles, as generally assumed[23,28]. We quantify future changes in bloom phenology by comparing present-day and future seasonal cycles of r and by attributing the difference to the terms in Equation 1 (i.e., calculating the budget).

For illustration, we focus on the subpolar North Atlantic, a region of intense spring blooms and the subject of many observational studies assessing the phenology of primary productivity. This region's typical seasonal cycle (Fig. 2a and 2b) entails increased surface Chl in late winter (r becomes positive in January/February in Fig. 2b) and a peak in May (first r zero-crossing after the initiation in Fig. 2b). Projected future shifts to earlier phytoplankton bloom initiation are characterized by a positive accumulation rate change (Δr; Δ indicates a change defined by future minus present day, Equation M5) in late winter (first gray shading periods in Fig. 2b, c). Conversely, at the bloom's peak, a lower accumulation rate under future conditions (negative Δr) suggests a shift to an earlier phasing (second gray shaded periods in Fig. 2b, c). Budget analysis for the accumulation rate change (Δr) reveals contributions from three terms: different changes in growth and loss rates ($\Delta\mu - \Delta l$), changes in temporal variations of ML depth ($-\Delta \mathrm{dln}h/\mathrm{dt}$), and changes in temporal variations of Chl:C ($\Delta \mathrm{dln}\theta/\mathrm{dt}$). The dominant terms for the positive Δr at bloom initiation (first gray shading period in Fig. 2) are positive anomalies of both $\Delta\mu - \Delta l$ caused by a higher growth rate ($\Delta\mu$) and temporal variations of ML depth ($-\Delta \mathrm{dln}h/\mathrm{dt}$, i.e., more gradually deepening ML) in January/February (Fig. 2c). As for peak bloom timing (second gray shading period), its earlier occurrence (i.e., negative Δr) results from a negative anomaly of $\Delta\mu - \Delta l$ mainly due to the reduced growth rate ($\Delta\mu$) in May.

By further decomposing the growth rate changes ($\Delta\mu$) into contributions from temperature-, nutrient-, and light-limitation (see Methods and Supplementary Note 2 for complete

expressions), we can attribute shifts in bloom timing to changes in environmental drivers (Fig. 2d). The change in the January/February growth rate, which sustains the earlier bloom initiation, is dominated by enhanced light availability due to the combination of shallower ML depth and increased surface irradiance (Fig. S5). A negative change in May's growth rate, which is the main cause of the earlier bloom peak, results from elevated nutrient- and temperature-limitation. Note that future projections of temperature changes in the subpolar North Atlantic can be negative, in contrast to other ocean domains ("warming hole")[24,40]. These results from the budget analysis of the subpolar North Atlantic are illustrated in the schematic in Figure 2e. At bloom initiation in January/February, positive future change in growth rate ($\Delta\mu$) due to improved light availability and reduced dilution by shallower winter ML ($-\Delta \mathrm{dln}h/\mathrm{dt}$) drive increases in Chl accumulation rate (Δr). Thus, the future accumulation rate becomes positive earlier than in the present-day climate, i.e., the bloom starts earlier. At peak bloom in May, negative future change in growth rate ($\Delta\mu$), due to colder temperature and lower nutrient concentrations, become the main cause of negative changes in the accumulation rate (Δr) in the future climate, although the loss rate will also decrease. The future negative accumulation rate anomaly indicates that the bloom peak (i.e., the timing of zero r) will occur earlier than that in preset-day.

Regional drivers of changes in phenology

The drivers of shifts in bloom initiation and bloom peak differ at the local (grid cell) scale and across biomes. In the eastern subarctic North Pacific, for example, unlike the subpolar North Atlantic, surface warming is the major driver for both earlier bloom initiation and earlier bloom peak (Extended Data Fig. 3). Warming elevates growth rates during bloom initiation and boosts predation pressure (loss rate) at bloom peak.

To understand the regional differences in processes that drive bloom phenological shifts, we estimate these processes' relative contributions to phenological shifts and show the dominant contributions within each biome (Fig. 3). The driving processes' relative contributions are calculated as the ratio between the time-integrated RHSs of the accumulation budget equation (Equation M5) and the time-integrated accumulation rate change, over the period between future and present-day bloom initiation/peak timings (Equation M6). In almost all ocean regions, contributions from changes in growth rates ($\Delta\mu$) and loss rates ($-\Delta l$) are the dominant terms of the accumulation rate changes (Fig. S6 and S7). Either of these changes alone could greatly alter bloom phenology. However, these two contributions nearly mirror each other, reflecting the fact that phytoplankton growth and predation by zooplankton are tightly coupled in this model. Previous studies have observed this tight coupling, and this mechanism plays an important role in explaining climatological features of the phytoplankton bloom as well as its interannual variability[22,23,28].

While phytoplankton growth and loss rates are tightly coupled, there are subtle differences between future changes in growth rate and those in loss rate (i.e., $\Delta\mu - \Delta l \neq 0$). This trophic level decoupling is the main mechanism for the peak bloom timing and initiation shifts in almost all ocean regions (Fig. 3a and 3c). In the oligotrophic mid-latitude oceans, the phytoplankton physiological response (temporal variations in Chl:C) is often the secondary, and sometimes the primary, process sustaining alterations in bloom peak timing (Fig. 3c and 3d), in agreement with previous results from observational and modeling studies focused on interannual time scales[41]. In parts of the Southern Ocean and the North Atlantic, changes in temporal ML variations (the dilution effect) strongly alter bloom initiation, reflecting the large projected forced ML depth changes (Fig. S5c). The anti-correlation of the contributions by temporal changes in ML depth and Chl:C reflects the physiology of photo-acclimation, by

231 which light-limited phytoplankton (i.e., deepening ML) increase intracellular Chl (i.e.,
232 increasing Chl:C) to maximize photosynthetic efficiency[42] (R=-0.43, p<0.01 for the initiation
233 in Fig. 3b, R=-0.56, p<0.01 for the peak timing in Fig. 3d; see also S6d, e and S7d, e).
234
235 Changing environmental drivers' contributions to future decoupling of phytoplankton growth
236 and loss ($\Delta\mu - \Delta l$) have distinct spatial footprints (Fig S8 and S9), with the dominant driver
237 varying among different ocean biomes (Fig. 4). Bloom initiation often occurs earlier due to
238 reduced light and temperature limitation of growth (Growth-L and Growth-T in Fig. 4a).
239 Elevated predation pressure arising from increased temperatures and biomass abundance cause
240 bloom peak timing to shift earlier (Loss-T and Loss-P in Fig. 4b, e.g., Northern Hemisphere
241 SPSS, STSS, ICE biomes). However, enhanced growth rates due to higher temperature
242 (Growth-T in Fig. 4b) can delay bloom peak (e.g., SA_STSS, SA_STPS, and SI_SPSS). In the
243 Arctic Ocean (N_ICE), where bloom phenology change emerges first, the main driver of earlier
244 initiation is enhanced light availability (Fig. 4a), as conceptually described in a previous study[43].
245 An earlier peak follows earlier initiation, as the bloom will experience stronger predation
246 pressure associated with abundant phytoplankton biomass and warmer temperatures in the
247 future (Fig. 4b).
248
249 **Discussion**
250 Warming operates as a major driver for future shifts in both bloom initiation and peak timing,
251 changing both growth and loss rates over most of the mid- to low latitudes and parts of the high
252 latitudes (Growth-T and Loss-T in Fig. 4). Notably, phytoplankton phenology shift drivers can
253 be distinct from general nutrient-limitation drivers of projected annual mean net primary
254 production changes within the same regions[44,45]. While at high latitudes growth rate changes
255 largely drive phase shifts in bloom initiation, increased predation pressure by zooplankton (top-

down control) plays an important role in altered bloom peak timing over much of the global ocean. It is important to note, particularly for observational studies, that identifying changes in bottom-up controls is a necessary but not sufficient condition for understanding phenology shifts, and that substantial roles for zooplankton, which are generally difficult to assess in observational studies, are a complementary and oftentimes necessary component.

Driver interdependence (e.g., stratification changes are almost always concurrent with surface warming and enhanced light availability) inherently limits correlation-based analysis for quantitatively attributing changes in bloom phenology. Our results indicate that light limitation is a primary control for future changes in bloom initiation only in limited regions (Growth-L in Fig. 4a). As such, the Sverdrup hypothesis, originally applied to explain year-to-year variability, cannot be generally extended to account for long-term shifts in bloom initiation. Light limitation changes are mediated through not only ML alterations (enhanced stratification) but also variable incident solar radiation at the sea surface, with regional dependence (Fig. S5).

Changes in phytoplankton bloom initiation and peak timing are spatially heterogenous (Fig. 1c, d), reflecting a delicate balance between the transient behavior of phytoplankton and individual underlying abiotic drivers. It should be noted that this study results are based on a single ESM, and that configurations and parameters of the biological component (e.g., the number of functional plankton groups and their couplings) are selected and tuned to reproduce the present-day climatological mean state of productivity based on representative field studies and ecological theory. Recent research has suggested that plankton community numbers and structures will respond to future climate change in spatially diverse ways[46,47]. In addition to more observational studies on the zooplankton-phytoplankton coupling, using more sophisticated ecological models in the next generation of ESMs could further deepen and

improve our understanding of the plankton community's phenological response to climate forcing.

Trophic level decoupling in response to anthropogenic forcing induces various future bloom phenological changes that result in both expanded and compressed future changes in net growth period length. Based on Northern Hemisphere high latitude oceans, our results diverge from research on the terrestrial biosphere, where phenological changes are anticipated to shift more uniformly to expanded growing seasons[9–13] as a forced response to anthropogenic warming and CO_2 fertilization. This remarkable contrast between land and sea reflects the fact that, in the ocean, anthropogenic warming triggers a number of processes that encompass both bottom-up and top-down drivers, with the balance between these drivers playing out quite differently in distinct ocean regions. The emergence of marine phytoplankton phenological change in high-productivity high-latitude ocean biomes indicates potential mismatches with the seasonal phasing of spawning in higher trophic levels, posing a potential risk to local marine ecosystems and ultimately the food security of populations dependent on marine resources.

Acknowledgements

R.Y., K.B.R., K.J.S., and A.T. were supported by the Institute for Basic Science (IBS), Republic of Korea, under IBS-R028-D1. S.S. acknowledges support from NSF's Southern Ocean Carbon and Climate Observations and Modeling (SOCCOM) Project under the NSF Award PLR-1425989, with additional support from NOAA and NASA Award NNX17AI75G. D.B. acknowledges support from NOAA under Ecosystem and Harmful Algal Bloom (ECOHAB) Award NA18NOS4780174. R.S. acknowledges support from NOAA (NA18OAR4320123). The authors thank Dr. Hyung-Gyu Lim for constructive suggestions on the manuscript. The authors also recognize the four reviewers' efforts and constructive

comments regarding how to improve the manuscript. ESM2M output analysis was conducted on the IBS/ICCP supercomputer "Aleph," 1.43 peta flops high-performance Cray XC50-LC Skylake computing system with 18,720 processor cores, 9.59 PB storage, and 43 PB tape archive space. High Performance Computing resources for the ESM2M Large Ensemble simulations themselves were provided by NOAA Oceanic and Atmospheric Research/Geophysical Fluid Dynamics Laboratory.

Author contributions

R.Y. and K.B.R. conceptualized the scientific framing of this study. R. Y. conducted all the analysis and wrote the initial draft of the manuscript. R.Y., K.B.R., A.T., K.J.S., S.S., D.B., and J.P.D. helped develop the scientific ideas and analytical methods, interpret the results, and write the final draft of the manuscript. The ESM2M simulations were performed by S.S. and R.S., and post-processing was provided by K.B.R.

Competing interests

The authors declare no competing interests.

Figure captions

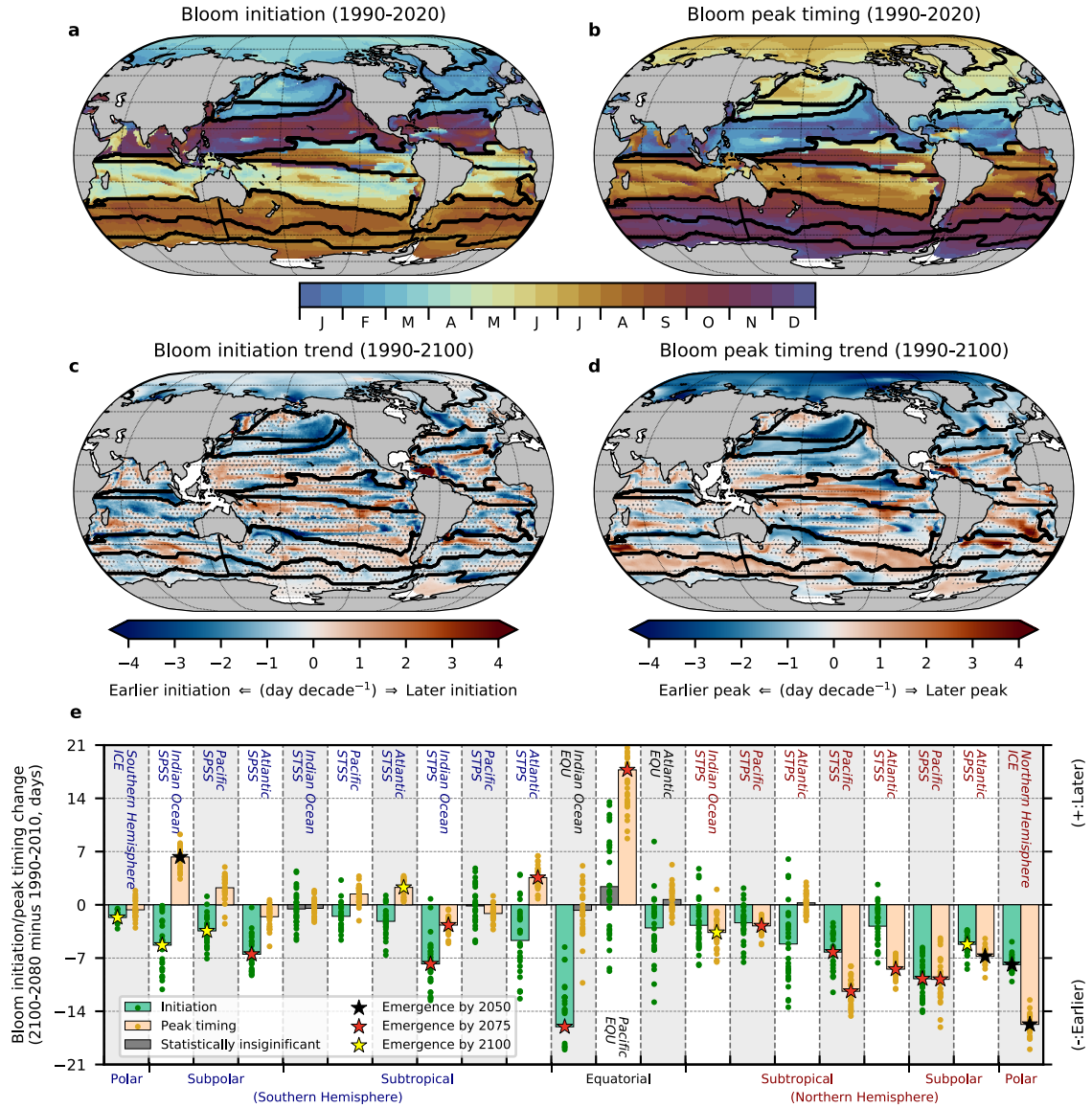

Fig. 1 | Projected future changes in the phytoplankton bloom phenology, and emergence timescales. a, b, Ensemble mean climatology (1990–2020) of phytoplankton bloom initiation and peak timing, simulated by the Geophysical Fluid Dynamics Laboratory Earth System Model 2 (GFDL-ESM2M) (letters indicate calendar month). **c, d,** Ensemble mean trends (1990–2100 under a Historical/RCP8.5 scenario) of bloom initiation and bloom peak timing. Positive trends indicate delayed initiation and delayed peak timing. Regions where the trend is statistically insignificant (at the 99% confidence level) are stippled. Black contours superimposed on the maps indicate biome boundaries. **E**, Biome-averaged changes (2080–2100 minus 1990–2010) in bloom initiation (green) and bloom peak timing (orange). In each ocean basin, subtropical seasonally stratified (STSS), subtropical permanently stratified (STPS), and equatorial (EQU) biomes are assigned in order from the pole (spatial map in Extend Data Figure 1). Ensemble mean changes are shown as bars, and dots on each bar represent the changes of 30 individual members. Stars at the end of a bar indicate that the ensemble mean changes will 'emerge', whereby the forced change exceeds the background internal variability by the end of 21st century (Methods). Base maps were made with Natural Earth and Cartopy[48].

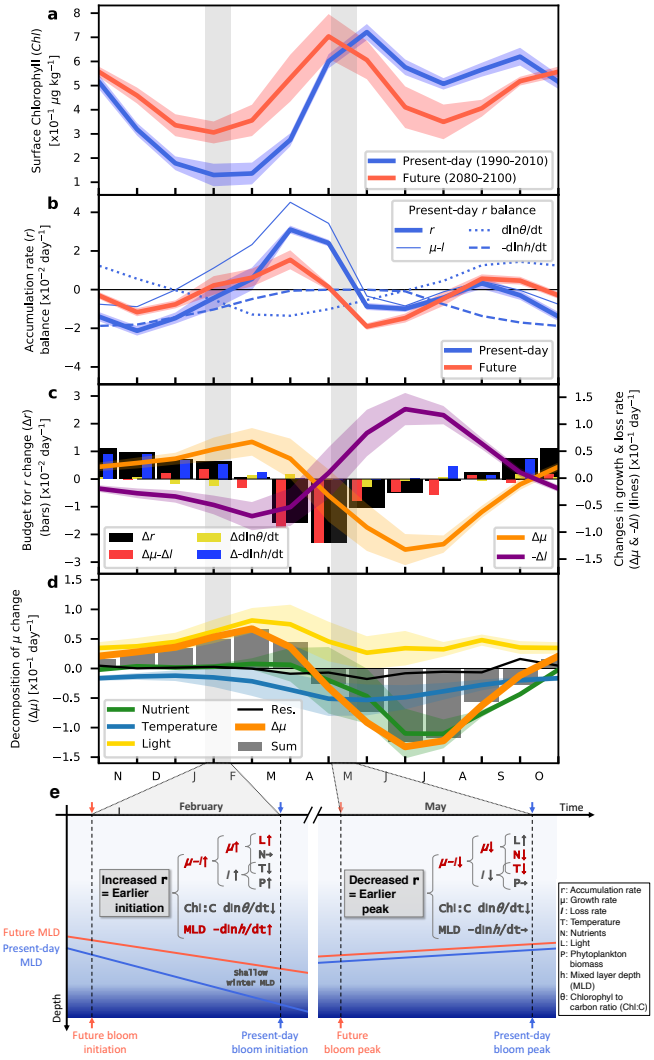

Fig. 2 | Mechanistic attribution of the bloom phenological changes for the subpolar North Atlantic (45°W, 55°N). a, Future (2080-2100) and present-day (1990-2010) annual cycles of surface chlorophyll concentration (*Chl*, g kg^{-1}), **b**, chlorophyll accumulation rate ($r \equiv \mathrm{d}\ln Chl/\mathrm{d}t$, day^{-1}) and its present-day term balance. r is determined by phytoplankton growth (μ) and loss rate (l), and temporal changes in Chl to Carbon ratio (θ) and mixed layer depth (h) (Equation 1). **c**, Budget for the accumulation rate changes (Δr, future r minus present-day r). The bars with respect to the left axis are accumulation rate change and three changes that drives the Δr (Equation M5). Changes in the growth and loss rates are also shown separately as lines with shading (right axis). **d**, Decomposition of the growth rate changes into changes in environmental drivers. The phytoplankton growth rate change is decomposed into changes in Temperature-, Nutrient-, Light-limitation (Equation M7). The periods commonly shaded in light gray in **a-d** represent the periods between the present-day and future bloom initiation/peak timing determined from the annual cycle of r (**b**). All line-shadings are the range of two standard deviations across the 30 ensemble members. **e**, Schematic figure for explaining the mechanisms for the bloom phenological shift. Dominant drivers of each change are highlighted by red.

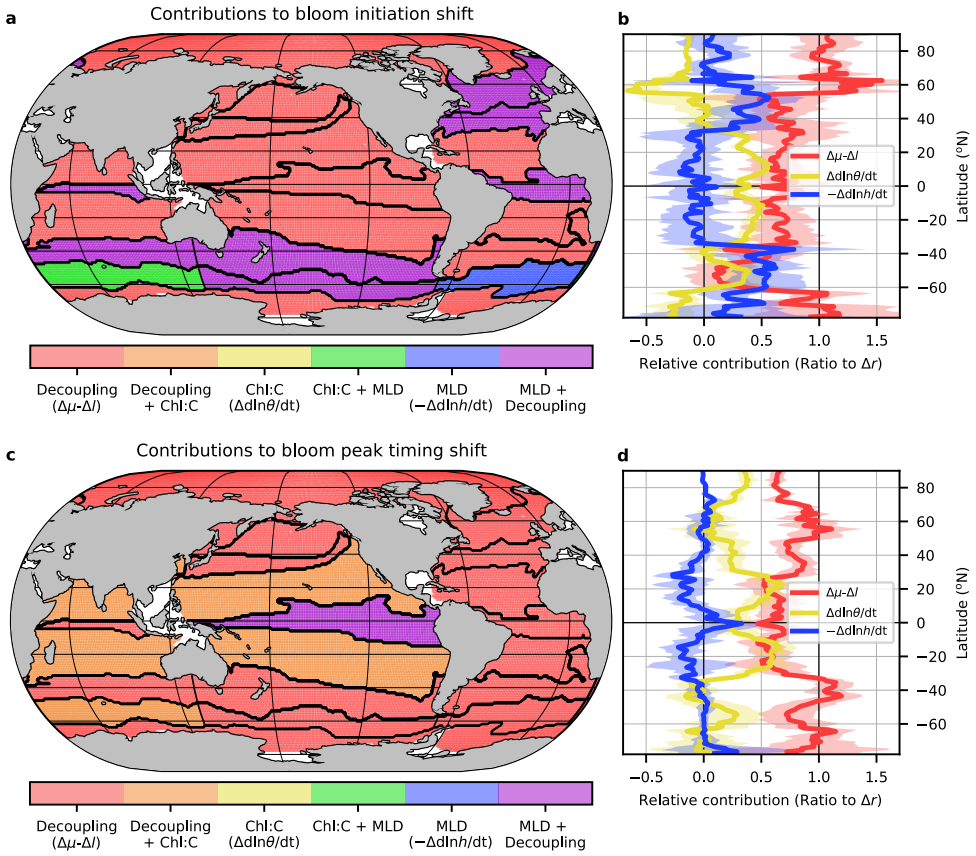

Fig. 3 | Dominant contribution(s) to shifts in bloom initiation and bloom peak timing. **a**, **c**, Largest contribution(s) to shifts in the bloom initiation and peak timing among the three driving processes (decoupling between changes in growth and loss rate; $\Delta\mu - \Delta l$, change in temporal variation in mixed layer depth (MLD); $-\Delta\, d\ln h/dt$, and change in Chl:C variation; $\Delta\, d\ln\theta/dt$) in each biome. The largest contributions are defined as the driving processes that dominantly support accumulation rate change (Δr) in more than 30 % of the biome area. **b**, **d**, Zonally averaged relative contributions of the three driving processes to the accumulation rate change. Line shadings indicate the range of two standard deviations across the 30 ensemble members. Base maps were made with Natural Earth and Cartopy[48].

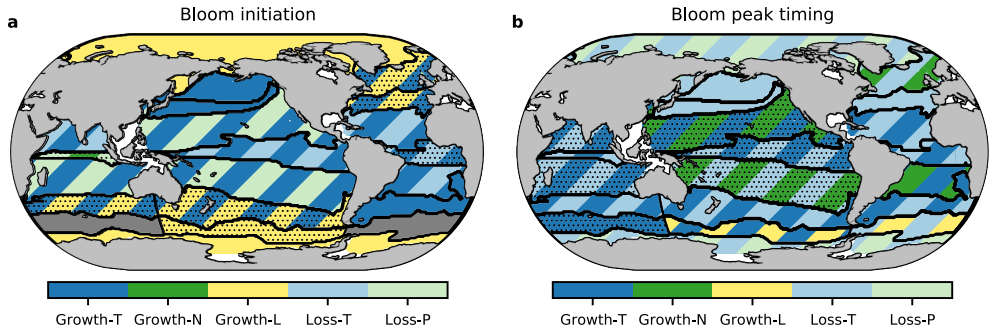

Fig. 4 | Environmental drivers that cause the future trophic level decoupling. Dominant environmental drivers that cause the decoupling of the future changes in phytoplankton growth ($\Delta\mu$) and loss rate ($-\Delta l$) **a,** at bloom initiation and **b,** at bloom peak. Growth-T, Growth-N, and Growth-L indicate that growth rate changes due to shifts in temperature, nutrient, and light, respectively, are the largest contributors to the decoupling in the biomes. Similarly, Loss-T and Loss-P show that loss rate changes due to altered temperature and biomass abundance, respectively, mainly contribute to the decoupling (i.e., $\Delta\mu - \Delta l \neq 0$). The dominant driver(s) in each biome is defined as the driver with changes that dominate the decoupling term ($\Delta\mu - \Delta l$) in more than 20 % of the biome area. If there are two dominant drivers, both are represented in stripes. Dots superimposed on biomes indicate regions where processes other than the decoupling (Chl:C variation changes or mixed layer variation change) are comparable to the contribution from the decoupling term in the accumulation rate budget, and dominant drivers in biomes where decoupling is not the main contributor to the phenological shift are gray shaded (c.f., Fig. 3a and 3c). Base maps were made with Natural Earth and Cartopy[48].

References

1. Bindoff, N. L. *et al.* Changing Ocean, Marine Ecosystems, and Dependent Communities. *IPCC Special Report on the Ocean and Cryosphere in a Changing Climate* 142 (2019).
2. Bopp, L. *et al.* Multiple stressors of ocean ecosystems in the 21st century: projections with CMIP5 models. *Biogeosciences* **10**, 6225–6245 (2013).
3. Fu, W., Randerson, J. T. & Moore, J. K. Climate change impacts on net primary production (NPP) and export production(EP) regulated by increasing stratification and phytoplankton communitystructure in the CMIP5 models. *Biogeosciences* **13**, 5151–5170 (2016).
4. Kwiatkowski, L. *et al.* Twenty-first century ocean warming, acidification, deoxygenation, and upper-ocean nutrient and primary production decline from CMIP6 model projections. *Biogeosciences* **17**, 3439–3470 (2020).
5. Cushing, D. H. Plankton Production and Year-class Strength in Fish Populations: an Update of the Match/Mismatch Hypothesis. In *Advances in Marine Biology* (eds. Blaxter, J. H. S. & Southward, A. J.) vol. 26 249–293 (Academic Press, 1990).
6. Durant, J., Hjermann, D., Ottersen, G. & Stenseth, N. Climate and the match or mismatch between predator requirements and resource availability. *Clim. Res.* **33**, 271–283 (2007).
7. Edwards, M. & Richardson, A. J. Impact of climate change on marine pelagic phenology and trophic mismatch. *Nature* **430**, 881–884 (2004).
8. Durant, J. M. *et al.* Contrasting effects of rising temperatures on trophic interactions in marine ecosystems. *Sci Rep* **9**, 15213 (2019).
9. Penuelas, J., Rutishauser, T. & Filella, I. Phenology Feedbacks on Climate Change. *Science* **324**, 887–888 (2009).
10. Ruosteenoja, K., Markkanen, T. & Räisänen, J. Thermal seasons in northern Europe in projected future climate. *Int J Climatol* **40**, 4444–4462 (2020).

11. Jeong, S.-J., Ho, C.-H., Gim, H.-J. & Brown, M. E. Phenology shifts at start vs. end of growing season in temperate vegetation over the Northern Hemisphere for the period 1982-2008: PHENOLOGY SHIFTS AT START VS. END OF GROWING SEASON. *Global Change Biology* **17**, 2385–2399 (2011).
12. Zhou, B., Zhai, P., Chen, Y. & Yu, R. Projected changes of thermal growing season over Northern Eurasia in a 1.5 °C and 2 °C warming world. *Environ. Res. Lett.* **13**, 035004 (2018).
13. Chen, M., Melaas, E. K., Gray, J. M., Friedl, M. A. & Richardson, A. D. A new seasonal-deciduous spring phenology submodel in the Community Land Model 4.5: impacts on carbon and water cycling under future climate scenarios. *Glob Change Biol* **22**, 3675–3688 (2016).
14. Kahru, M., Brotas, V., Manzano-Sarabia, M. & Mitchell, B. G. Are phytoplankton blooms occurring earlier in the Arctic?: PHYTOPLANKTON BLOOMS IN THE ARCTIC. *Global Change Biology* **17**, 1733–1739 (2011).
15. Marchese, C. *et al.* Changes in phytoplankton bloom phenology over the North Water (NOW) polynya: a response to changing environmental conditions. *Polar Biol* **40**, 1721–1737 (2017).
16. Friedland, K. D. *et al.* Phenology and time series trends of the dominant seasonal phytoplankton bloom across global scales. *Global Ecol Biogeogr* **27**, 551–569 (2018).
17. Winder, M. & Sommer, U. Phytoplankton response to a changing climate. *Hydrobiologia* **698**, 5–16 (2012).
18. Asch, R. G., Stock, C. A. & Sarmiento, J. L. Climate change impacts on mismatches between phytoplankton blooms and fish spawning phenology. *Glob Change Biol* **25**, 2544–2559 (2019).

19. Henson, S., Cole, H., Beaulieu, C. & Yool, A. The impact of global warming on seasonality of ocean primary production. *Biogeosciences* **10**, 4357–4369 (2013).
20. Henson, S. A., Cole, H. S., Hopkins, J., Martin, A. P. & Yool, A. Detection of climate change-driven trends in phytoplankton phenology. *Glob Change Biol* **24**, e101–e111 (2018).
21. Hashioka, T., Sakamoto, T. T. & Yamanaka, Y. Potential impact of global warming on North Pacific spring blooms projected by an eddy-permitting 3-D ocean ecosystem model. *Geophysical Research Letters* **36**, (2009).
22. Behrenfeld, M. J. & Boss, E. S. Resurrecting the Ecological Underpinnings of Ocean Plankton Blooms. *Annu. Rev. Mar. Sci.* **6**, 167–194 (2014).
23. Behrenfeld, M. J. Climate-mediated dance of the plankton. *Nature Clim Change* **4**, 880–887 (2014).
24. Schlunegger, S. *et al.* Time of Emergence and Large Ensemble Intercomparison for Ocean Biogeochemical Trends. *Global Biogeochem. Cycles* **34**, (2020).
25. Sverdrup, H. U. On Conditions for the Vernal Blooming of Phytoplankton. *ICES Journal of Marine Science* **18**, 287–295 (1953).
26. Sommer, U. & Lewandowska, A. Climate change and the phytoplankton spring bloom: warming and overwintering zooplankton have similar effects on phytoplankton. *Global Change Biology* **17**, 154–162 (2011).
27. Behrenfeld, M. J. Abandoning Sverdrup's Critical Depth Hypothesis on phytoplankton blooms. *Ecology* **91**, 977–989 (2010).
28. Behrenfeld, M. J., Doney, S. C., Lima, I., Boss, E. S. & Siegel, D. A. Annual cycles of ecological disturbance and recovery underlying the subarctic Atlantic spring plankton bloom. *Global Biogeochem. Cycles* **27**, 526–540 (2013).

29. Arteaga, L. A., Boss, E., Behrenfeld, M. J., Westberry, T. K. & Sarmiento, J. L. Seasonal modulation of phytoplankton biomass in the Southern Ocean. *Nat Commun* **11**, 5364 (2020).
30. Behrenfeld, M. J. & Boss, E. S. Student's tutorial on bloom hypotheses in the context of phytoplankton annual cycles. *Glob Change Biol* **24**, 55–77 (2018).
31. Schlunegger, S. *et al.* Emergence of anthropogenic signals in the ocean carbon cycle. *Nat. Clim. Chang.* **9**, 719–725 (2019).
32. Dunne, J. P. *et al.* GFDL's ESM2 Global Coupled Climate–Carbon Earth System Models. Part II: Carbon System Formulation and Baseline Simulation Characteristics*. *Journal of Climate* **26**, 2247–2267 (2013).
33. Dunne, J. P. *et al.* GFDL's ESM2 Global Coupled Climate–Carbon Earth System Models. Part I: Physical Formulation and Baseline Simulation Characteristics. *Journal of Climate* **25**, 6646–6665 (2012).
34. Rodgers, K. B., Lin, J. & Frölicher, T. L. Emergence of multiple ocean ecosystem drivers in a large ensemble suite with an Earth system model. *Biogeosciences* **12**, 3301–3320 (2015).
35. Cabré, A., Shields, D., Marinov, I. & Kostadinov, T. S. Phenology of Size-Partitioned Phytoplankton Carbon-Biomass from Ocean Color Remote Sensing and CMIP5 Models. *Front. Mar. Sci.* **3**, (2016).
36. Ji, R., Edwards, M., Mackas, D. L., Runge, J. A. & Thomas, A. C. Marine plankton phenology and life history in a changing climate: current research and future directions. *Journal of Plankton Research* **32**, 1355–1368 (2010).
37. Henson, S. A., Beaulieu, C. & Lampitt, R. Observing climate change trends in ocean biogeochemistry: when and where. *Glob Change Biol* **22**, 1561–1571 (2016).

38. Hegerl, G. C. *et al.* Detecting greenhouse-gas-induced climate change with an optimal fingerprint method. *Journal of Climate* **9**, 2281–2306 (1996).

39. Massonnet, F. *et al.* Constraining projections of summer Arctic sea ice. *The Cryosphere* **6**, 1383–1394 (2012).

40. Chemke, R., Zanna, L. & Polvani, L. M. Identifying a human signal in the North Atlantic warming hole. *Nat Commun* **11**, 1540 (2020).

41. Behrenfeld, M. J. *et al.* Revaluating ocean warming impacts on global phytoplankton. *Nature Clim Change* **6**, 323–330 (2016).

42. Geider, R., MacIntyre, H. & Kana, T. Dynamic model of phytoplankton growth and acclimation: responses of the balanced growth rate and the chlorophyll a:carbon ratio to light, nutrient-limitation and temperature. *Mar. Ecol. Prog. Ser.* **148**, 187–200 (1997).

43. Wassmann, P. & Reigstad, M. Future Arctic Ocean Seasonal Ice Zones and Implications for Pelagic-Benthic Coupling. *Oceanog.* **24**, 220–231 (2011).

44. Laufkötter, C. *et al.* Drivers and uncertainties of future global marine primary production in marine ecosystem models. *Biogeosciences* **12**, 6955–6984 (2015).

45. Nakamura, Y. & Oka, A. CMIP5 model analysis of future changes in ocean net primary production focusing on differences among individual oceans and models. *J Oceanogr* **75**, 441–462 (2019).

46. Marinov, I., Doney, S. C. & Lima, I. D. Response of ocean phytoplankton community structure to climate change over the 21st century: partitioning the effects of nutrients, temperature and light. *Biogeosciences* **7**, 3941–3959 (2010).

47. Henson, S. A., Cael, B. B., Allen, S. R. & Dutkiewicz, S. Future phytoplankton diversity in a changing climate. *Nat Commun* **12**, 5372 (2021).

48. Elson, P. et al. SciTools/cartopy: v0.20.2. *Zenodo* https://doi.org/10.5281/zenodo.1182735 (2022).

508

Methods

Model and observational data

The 30-member ensemble simulation used in this study applied the Geophysical Fluid Dynamics Laboratory Earth System Model 2 (GFDL-ESM2M[32,33]) to historical (1950–2005) and RCP8.5 (2006–2010) pathways between 1950 and 2100. The initial conditions (the 1st January 1950 conditions) for ensemble member 2–30 are the January 2nd–30th model states of the first ensemble member. The model runs presented here share initial conditions, model version, and forcing with a previous study[34] but differ in that they were performed on a separate computing architecture (and with more extensive high-frequency ocean model output saved). The members therefore differ from one another regarding variability mode phasing for a given time-slice, but not in their mean state evolution or statistical characteristics. The ocean biogeochemical component of ESM2M (Tracers of Ocean Phytoplankton with Allometric Zooplankton code version 2; TOPAZ2) has three phytoplankton groups ("small," "large," and diazotrophic phytoplankton) plus one implicit allometric zooplankton group and explicitly calculates a chlorophyll-to-carbon ratio (Chl:C) from background light, nutrient, and temperature conditions. ESM2M and other CMIP5 models, with ocean biogeochemistry observations, have been compared using historical[49] and RCP8.5[2] simulations. We used daily means of surface Chl concentrations (g kg^{-1}) to detect future changes in bloom timing and monthly outputs of other ocean physical and biogeochemical fields for more extensive budget calculations over the 1990–2100 time period.

We also used a satellite-derived daily sea surface Chl product[50] to validate the model representations of phytoplankton bloom phenology. Data missing from the observational record due to cloud cover are linearly interpolated along the time axis, except for data gaps that last more than 14 days (mostly due to the polar night).

To ensure a fair comparison between the model output and the observations, after the original model outputs were regridded to spatiotemporal resolution of the observations (daily, 1° latitude x 1° longitude), we created 30-member resampled model outputs by resampling only the regridded model data where observations exist. All model-observation comparisons (Fig. S1–S3) use the 30-member resampled model outputs, unless otherwise noted.

Comparisons of modeled and observed surface Chl concentrations' annual cycle for each biome are shown in Figure S1 and S2. Biomes are defined partly by following a previously published method[51] that classifies ocean regions based on physical and biogeochemical environmental factors. Here, in order for the biome classifications to reflect the phenological characteristics of the phytoplankton bloom, bloom peak timing was used to determine biome boundaries, as an additional constraint on the variables originally used (sea ice concentration, surface Chl, mixed layer (ML) depth, and sea surface temperature). In order from the pole, each basin except for the North Indian Ocean has ice (ICE), subpolar seasonally stratified (SPSS), subtropical seasonally stratified (STSS), subtropical permanently stratified (STPS), and equatorial (EQU) biomes (map in Extended Data Fig. 1). Biomes are defined using present-day climatologies, and their boundaries are not time-varying.

Phytoplankton bloom definition

To calculate phytoplankton bloom initiation and peak timing, we apply the accumulation rate (r)-based framework[30] to daily surface Chl concentration data (i.e., $r \equiv \frac{d\ln(Chl)}{dt}$). We use the surface Chl concentration values (g kg^{-1}) rather than depth-integrated values (g) in order to compare a broadly observable and well-established quantity provided by satellite measurements, and we further assume that surface concentrations are indicative of the entire

559 mixed layer. In our framework using surface/mixed layer concentrations, the temporal
560 variation in the mixed layer depth must be explicitly considered in quantifying its seasonal
561 variation (derived in a subsequent section of Methods). The total vertically-integrated
562 phytoplankton biomass has also been previously used as a metric of phytoplankton seasonality
563 to explain the drivers from observational datas [22,29,52].
564
565 In an annual cycle, bloom initiation is defined as the day of the year when the accumulation
566 rate becomes positive, and the bloom peak is defined as the day of the year, after the initiation,
567 when the accumulation rate returns to negative. The difference between the peak and the
568 initiation is the net growth period length. In practice, to avoid artificial bloom timing jumps
569 due to discontinuities at the start of a 365-day calendar year, the annual cycle is defined as
570 twelve months centered around the maximum day of climatological surface Chl in the annual
571 calendar cycle at each grid point. We first obtain the bloom peak timing and bloom magnitude
572 (Chl value at the peak) within the annual cycle at each grid point. We then use the
573 corresponding accumulation rate (r) time series to back-search for consecutive 14-day intervals
574 with negative accumulation, representing non-bloom periods. We define the transition from a
575 bloom period (positive r) to a non-bloom period (negative r) as the bloom initiation. All daily
576 data from the model and observations were low-passed filtered by a Lanczos filter with a 21-
577 day half power period before we calculated bloom timings, to remove the phytoplankton's
578 transient spike response to atmospheric storm timescales (~a week) and ocean sub-mesoscale
579 perturbations (~ few weeks) that are not the targets of this study.
580
581 When there are more than two peaks of surface Chl in an annual cycle, we chose the "spring
582 bloom" as the grid point bloom, which generally starts after the winter convection and thus the
583 above assumption of identity between surface and ML-averaged Chl reasonably holds. To do

584 this, we imposed an additional condition in only the region with a pronounced seasonal cycle
585 in surface Chl the bloom should peak between January to July north of 40° and between July
586 and January south of 30º. As a result, the blooms identified are consistent between the model
587 and observations (Fig. S3).
588
589 **Time of Emergence calculation**
590 We invoke the "Time of Emergence (ToE)" concept to estimate when an anthropogenically
591 forced trend (signal) exceeds background internal variability (noise) using the large number of
592 realizations (30 members) available for the identical forcing climate trajectory from the Large
593 Ensemble simulation. For the yearly time series of bloom metrics (initiation, peak timing, and
594 magnitude), the signal is calculated as the ensemble mean of 30 trends and the noise as the
595 standard deviation of these trends. We follow the widespread assumption with Large Ensemble
596 simulations that modeled internal variability across all timescales is normally distributed about
597 the mean climate state. We used the standard two-sided *t*-test to evaluate whether a forced
598 signal is outside the range of internal variability. When the signal magnitude is twice that of
599 the noise, the null hypothesis (i.e. that the signal is due to internal variability) is rejected with
600 95% confidence; that is, the anthropogenically forced trend extends beyond the range of
601 background internal variability[31]. The signal-to-noise ratio is calculated iteratively with a fixed
602 starting reference year of 1990, and the ToE is defined as the first year when the ratio is larger
603 than 2. In this study, the ToE is estimated from biome-averaged yearly time series of bloom
604 metrics (Extended Data Fig. 1 and S4). The area aggregation of time series reduces noise and
605 thus promotes signal detection, as has been previously noted[20].
606
607 **Accumulation rate budget analysis**

Under the assumption that Chl advection and diffusion terms are negligible over spatial and temporal scales of ~100 km and ~1 month, respectively, we begin with the conservation equation for phytoplankton biomass (P_i, g C kg^{-1}) in the ML:

$$\frac{dP_i h}{dt} = (\mu_i - l_i)\, P_i h \tag{M1}$$

to derive an equation for computing the budget of Chl accumulation rate, where μ, l, and h indicate the phytoplankton growth rate (day^{-1}), loss rate (day^{-1}), and ML depth (m), respectively, and the subscript i represents phytoplankton groups in the model (small phytoplankton, large phytoplankton, and diazotrophic phytoplankton in TOPAZ2). Subsequently, the conservation equation is rewritten as a vertical one-dimensional phytoplankton biomass equation:

$$\frac{dP_i}{dt} = (\mu_i - l_i)\, P_i - \frac{P_i}{h}\frac{dh}{dt}. \tag{M2}$$

Assuming the water is well mixed within the ML, the surface biomass concentration is identical to that averaged throughout the ML. Under the assumption, sea surface biomass concentration can vary with growth (cell division) and loss (zooplankton grazing, aggregation, mortality, etc.) in the ML. Additionally, biomass-free water entraining from below, through ML deepening, can dilute surface/ML biomass concentration (dilution effect). Here, the effect is parameterized as follows:

$$\frac{dh}{dt} = \begin{cases} \frac{dh}{dt} & \left(\frac{dh}{dt} > 0; deepening\right) \\ 0 & \left(\frac{dh}{dt} \leq 0; shoaling\right) \end{cases}. \tag{M3}$$

It should be noted that, in ocean regions where phytoplankton accumulate below the mixed layer in the warming season (as with subsurface Chlorophyll maxima), this simplification might lead to large errors throughout the season when the mixed layer deepens (from autumn to winter). Using the chlorophyll to carbon ratio ($\theta_i = \frac{Chl_i}{P_i}$), the phytoplankton biomass equation can be rewritten as the equation for Chl accumulation rate (Equation 1 in the Main text),

$$\frac{d\ln(Chl)}{dt} \equiv r = \sum_{i=1}^{3}\left((\mu_i - l_i) + \frac{d\ln(\theta_i)}{dt}\right)\gamma_i - \frac{d\ln(h)}{dt}, \quad \text{(M4)}$$

where Chl is the sum of the chlorophyll concentration of three groups ($chl = \sum_{i=1}^{3} Chl_i$), and γ_i represents the concentration ratio of each group ($\gamma_i = Chl_i/Chl$). For convenience, in the main text, summations of growth and loss rate changes and Chl:C variations over the three phytoplankton groups are expressed without the subscript i.

Based on this equation, accumulation rate changes from the present-day to the future (Δr) are described as the sum of three terms: the changes in growth rate and loss rate, the time rate of change in the Chl:C, and the time rate of change in the ML depth,

$$\begin{aligned}\Delta r &= \sum_{i=1}^{3}\Delta(\gamma_i\mu_i) + \sum_{i=1}^{3}\Delta(\gamma_i l_i) + \sum_{i=1}^{3}\Delta\left(\gamma_i\frac{d\ln(\theta_i)}{dt}\right) - \Delta\frac{d\ln(h)}{dt} \\ &\equiv (\Delta\mu - \Delta l) + \Delta\frac{d\ln(\theta)}{dt} - \Delta\frac{d\ln(h)}{dt}.\end{aligned} \quad \text{(M5)}$$

All terms in the accumulation rate budget analysis are calculated at individual grid points before being aggregated across biomes.

Equation M5 estimates relative contributions from processes that drive bloom phenological shifts (i.e., changing accumulation rates). The relative contributions of the driving processes are calculated as the ratio of the time-integrated RHSs of Equation M5 to the time-integrated accumulation rate change over the period between future and present-day bloom initiation/peak timing (gray shaded periods in Fig. 2a–d):

$$\frac{\int_{t_0}^{t_1}(\Delta\mu-\Delta l)\,dt}{\int_{t_0}^{t_1}\Delta r\,dt} + \frac{\int_{t_0}^{t_1}\left(\Delta\frac{d\ln(\theta)}{dt}\right)dt}{\int_{t_0}^{t_1}\Delta r\,dt} + \frac{\int_{t_0}^{t_1}\left(-\Delta\frac{d\ln(h)}{dt}\right)dt}{\int_{t_0}^{t_1}\Delta r\,dt} = 1, \quad \text{(M6)}$$

where $t_0$and t_1 are the earlier and later days in the year, respectively, among future bloom initiation/peak and present-day bloom initiation/peak.

Decomposition of growth/loss rate change

In the TOPAZ2 biogeochemical component of ESM2M, the phytoplankton growth rate is a function of temperature, nutrient, and light limitation terms (T^{lim}, N^{lim}, and L^{lim}), and the loss rate is described as a function of temperature limitation and phytoplankton biomass abundance (T^{lim} and P_i). Increases in water temperature, light levels, and nutrient concentrations promote phytoplankton growth, and rising water temperature and phytoplankton biomass themselves enhance phytoplankton loss, mainly by augmenting zooplankton predation pressure. Model parameters are assigned to each phytoplankton group and then the limitation terms are calculated separately. The Taylor expansions of the total growth rate ($\Delta\mu$) and loss rate (Δl) are expressed as contributions from changes in temperature-, light-, and nutrients-limitation (for $\Delta\mu$) and temperature-limitation and biomass (for Δl) (See also Supplementary Note 2):

$$\Delta\mu = \sum_{i=1}^{3}\Delta(\gamma_i\mu_i) \approx \sum_{i=1}^{3}\gamma_i\frac{\partial\mu_i}{\partial T^{lim}}\Delta T^{lim} + \sum_{i=1}^{3}\gamma_i\frac{\partial\mu_i}{\partial N_i^{lim}}\Delta N_i^{lim} + \sum_{i=1}^{3}\gamma_i\frac{\partial\mu_i}{\partial L_i^{lim}}\Delta L_i^{lim} + \text{Residual}, \quad \text{(M7)}$$

$$\Delta l = \sum_{i=1}^{3}\Delta(\gamma_i l_i) \approx \sum_{i=1}^{3}\gamma_i\frac{\partial l_i}{\partial T^{lim}}\Delta T^{lim} + \sum_{i=1}^{3}\gamma_i\frac{\partial l_i}{\partial P_i}\Delta P_i + \text{Residual}. \quad \text{(M8)}$$

Residuals in the above equations include contributions from changes in the chlorophyll concentration ratio (γ_i) and other higher-order terms, but these tend to be minor overall (Fig. S8 and S9). Partial derivatives of the growth rate with respect to temperature-, nutrients-, and light-limitation, and of the loss rate with respect to temperature-limitations and biomass, are computed analytically using model equations (Supplementary Note 2).

Data availability

The 30-member GFDL-ESM2M ensemble simulations[53] used in this study are available through the data transfer service Globus (https://www.globus.org). In the server (http://poseidon.princeton.edu), daily surface ocean variables are available under:

/GFDL_ESM2M/ENSEMBLE_RCP85/OCN/OCN_1D_1x1/ and monthly mean ocean fields are under /GFDL_ESM2M/ENSEMBLE_RCP85/OCN/OCN_1M_1x1. The MODIS-Aqua Level-3 Binned Chlorophyll Data[50] are available at https://oceancolor.gsfc.nasa.gov.

Code availability

The codes used to analyze data and generate all figures are based on Python with associated standard Python packages (Xarray, NumPy, SciPy, Matplotlib, Cartopy, etc.). The codes[54] are available from https://doi.org/10.5281/zenodo.6301884.

References

49. Frölicher, T. L. *et al.* Dominance of the Southern Ocean in Anthropogenic Carbon and Heat Uptake in CMIP5 Models. *Journal of Climate* **28**, 862–886 (2015).
50. NASA Ocean Biology Processing Group. MODIS-Aqua Level 3 Binned Chlorophyll Data Version R2018.0. (2017) doi:10.5067/AQUA/MODIS/L3B/CHL/2018.
51. Fay, A. R. & McKinley, G. A. Global open-ocean biomes: mean and temporal variability. *Earth Syst. Sci. Data* **6**, 273–284 (2014).
52. Behrenfeld, M. J., Doney, S. C., Lima, I., Boss, E. S. & Siegel, D. A. Reply to a comment by Stephen M. Chiswell on: "Annual cycles of ecological disturbance and recovery underlying the subarctic Atlantic spring plankton bloom" by M. J. Behrenfeld et al. (2013): REPLY. *Global Biogeochem. Cycles* **27**, 1294–1296 (2013).
53. Geophysical Fluid Dynamics Laboratory Earth System Model 2 (GFDL-ESM2M) 30-member ensemble simulations, historical (1950–2005) and RCP8.5 (2006–2010) scenario, http://poseidon.princeton.edu (2019).

692 54. Yamaguchi, R. Notebooks for "Trophic level decoupling drives future change in
693 phytoplankton bloom phenology" by Yamaguchi et al. (2022). Zenodo,
694 https://doi.org/10.5281/zenodo.6301884 (2022).
695